Energetics of neutral Si dopants in InGaAs: An *ab initio* and semiempirical Tersoff model study

Cheng-Wei Lee,[1] Binit Lukose,[2] Michael O. Thompson,[1] and Paulette Clancy[2,*]

[1]*Department of Materials Science and Engineering, Cornell University, Ithaca, New York 14853, USA*

[2]*School of Chemical and Biomolecular Engineering, Cornell University, Ithaca, New York 14853, USA*

(Received 23 October 2014; revised manuscript received 31 December 2014; published 16 March 2015)

A roadblock in utilizing III-V semiconductors for scaled-down electronic devices is their poor dopant activation. As a first step to unravel the dopant behavior in InGaAs, we studied the tendency for dopant formation computationally using two approaches: *ab initio* and semiempirical methods. We studied a number of structural possibilities, such as the impact of local sites and local and global environments. We will show that the dopant we considered here, Si, has discrete preferences for certain sites and the nature of its surroundings. Substitutional defects are clearly preferred over interstitial locations. We shall show that cation ordering has an impact on dopant energetics. Critically, for large-scale simulations of dopant diffusion in InGaAs alloys, we also present a parameterization of the Abell-Tersoff semiempirical potential for pairwise interactions between silicon atoms and each of the elements constituting InGaAs. In the absence of experimental data, reference parameters for estimating the Tersoff values were obtained using *ab initio* pseudopotential calculations (density functional theory and generalized gradient approximations). These sets of Tersoff parameters were optimized to describe the bulk structural properties of the mostly theoretical alloys Si-As, Si-Ga, and Si-In. We demonstrate the transferability of these parameters by predicting formation energies of extrinsic point "defects" of Si on a variety of sites in ternary InGaAs alloys with different local compositional configurations, both random and ordered. Tersoff model predictions of the extrinsic "substitution energy" of a Si dopant on a cationic lattice site were found to be independent of the composition of the dopant's second nearest neighbors, but were affected by the strain induced by a local arrangement of In and Ga cationic atoms. This finding is important since common deposition processes used to create InGaAs may lead to specifically ordered patterns within the cation sublattice.

DOI: 10.1103/PhysRevB.91.094108 PACS number(s): 61.72.uj, 12.39.Pn, 71.15.Dx, 71.10.−w

I. INTRODUCTION

III-V compound semiconductors exhibit a wide range of properties enabling devices from narrow band detectors to wide band gap high-temperature electronics. Recently, there has been renewed interest in the use of III-V based materials as replacements for silicon devices to enable continued progress along Moore's Law. In particular, the ternary alloy $In_xGa_{1-x}As$ ($x \approx 0.47$) is considered to be a very promising candidate with a suitable balance between its reduced band gap, high carrier mobility, and low density of interface states. With a band gap near 0.75 eV and an electron mobility above $8000\,cm^2/V-s$ [1], InGaAs promises to address both speed and power challenges in next-generation devices. As mentioned in a 2010 presentation by Intel's Director of Technology Strategy, Paolo Gargini, "the inclusion of III-V materials is a 2015 transistor option that could deliver either three times the performance of silicon at the same power consumption, or deliver the same performance as silicon at one-tenth the power consumption" [2].

In the past, III-V materials have been difficult to integrate at Si densities due to the absence of a native oxide having a low density of defect states, and also due to the pinning of the Fermi-level at a SiO_2 interface. These issues have become less critical with the shift to metal gates and high-k dielectric gate stacks. Recent improvements in these interfaces have led to the incorporation of InGaAs into the 2012 International Technology Roadmap for Semiconductors (ITRS) [3], which suggested possible implementation as early as 2015 in the 11 nm nodes.

However, there are substantial issues in the integration of InGaAs into conventional device process flows. Traditional III-V devices are based on vertical geometries with dopant profiles that can be introduced during molecular beam epitaxy (MBE) or chemical vapor deposition (CVD) growth [4–6]. However, the lateral impurity doping profiles required for planar devices will, most likely, be generated by ion implantation and require some form of thermal activation. Silicon is the leading candidate as an *n*-type dopant, and it is critical that this activation process be optimized through suitable annealing conditions. Preliminary experimental data have shown that the activation of Si is unexpectedly challenging requiring temperatures above 600 °C, which may impact gate and contact integrity. Even at these temperatures, the concentration of activated dopants is low, resulting in high parasitic resistivity. In addition, the diffusion of Si at these temperatures is extremely limited as evidenced by secondary ion mass spectrometry (SIMS) [7]. To resolve these issues, it is critical to gain a fundamental understanding of the limitations to dopant activation and to understand kinetics of impurity transport. This is the motivation for the present computational paper.

We approach this dopant activation issue in two ways. First, we use first principles (*ab initio*) methods to determine the relative energy for Si to reside on substitutional cation sites, rather than anion sites. Although dopant activation can be associated with charged dopant states, we limit our current studies to the study of neutral defects in the system, since this is the only charge state that can be studied using semiempirical models. Second, given an experimentally known driving force for Si to occupy cation sites for some processing conditions, we hypothesize that the migration of Si atoms is kinetically restricted by local atomic environments, such that Si cannot

*Paulette.Clancy@cornell.edu

 ©2015 American Physical Society

diffuse to cation sites. We investigate this by calculating the total energies of all possible atomic configurations surrounding Si atoms within a second nearest neighbor (2nn) distance. Given that we are considering a ternary host matrix, the number of possible unique arrangements of neighbors is extremely large. Since first principles methods remain too computationally expensive to solve such combinatorial problems, we turn to semiempirical models, such as the Tersoff potential model, to describe the interactions between pairs of atoms. The much higher computational efficiency of such models allows us to undertake larger-scale molecular simulations containing thousands of atoms that can more realistically capture the transport of Si dopants in the InGaAs matrix. Fortunately, suitable Tersoff models exist for the III-V materials, both the elemental systems (In-In [8], Ga-Ga [8], As-As [8]) and all the unlike pairs of atom types, e.g., Ga-As [8]). However, there are no Tersoff models for the Si$-X$ interactions (where $X =$ In, Ga, or As). Hence, we develop and test suitable Tersoff models in this paper.

The Tersoff potential model was originally developed for Si [9–11] and later extended to Ge and SiC by Tersoff [12]. Tersoff models fall into the category of "bond order" potentials originally suggested by Abell, in which the two-body potential depends on the environment of the neighboring atoms. Like the Stillinger-Weber model, the Tersoff potential was developed for covalently bonded systems.

Extension of the Tersoff model to describe III-V alloys has been reasonably widespread: Smith developed Tersoff parameters for the simulation of atomic collisions in GaAs [13]. The first set of Tersoff parameters for AlAs was developed by Sayed *et al.* [14]. Extension to InAs was made by Ashu *et al.* [15] for studies of ion bombardment, and further modified by Nordlund *et al.* [16]. A comprehensive set of Tersoff parameters for many III-V materials of technological interest was developed by Powell *et al.* [17] for application of quantum dot optoelectronics. Tersoff parameters for In-As and Ga-As were also developed by Hammerschmidt *et al.* [8], which are used for our application here. Of more direct importance to our interest in doped InGaAs materials, Detz and Strasser [18] recently tested Tersoff models for InGaAs, InAlAs, and GaAsSb for their ability to reproduce elastic properties, as well as predict bulk and shear moduli.

In this paper, we will briefly describe the Tersoff potential model (providing more background details in the

TABLE I. Equilibrium bulk properties of Si-X interactions from *ab initio* (DFT/GGA) and semiempirical (Tersoff model) calculations.

Si-As

Crystal structure	E_{coh}(eV)			Bond length (Å)			B (GPa)		
	GGA	ps.1	ps.2	GGA	ps.1	ps.2	GGA	ps.1	ps.2
ZnS	4.70	4.71	4.71	2.48	2.47	2.44	49	49	56
NaCl	4.88	4.85	4.86	2.61	2.65	2.64	93	74	82
CsCl	4.51	4.53	4.57	2.81	2.81	2.84	77	87	94
ZnO[a,b]	4.85	4.71	4.71	2.43; 2.75	2.47; 2.47	2.44; 2.44	60	49	56
NiAs[b]	4.84	4.67	4.77	2.63	2.67	2.65	84	89	87
h-BN[a,c]	4.86	4.68	4.78	2.51; 2.60	2.54; 2.63	2.52; 2.61	71	56	68

Si-Ga

Crystal structure	E_{coh}(eV)		Bond length (Å)		B (GPa)	
	GGA	ps.1 & 2	GGA	ps.1 & 2	GGA	ps.1 & 2
ZnS	3.85	3.85	2.45	2.44	76	58
NaCl	3.84	3.84	2.62	2.65	64	79
CsCl	3.77	3.79	2.81	2.80	61	102
ZnO	3.82	3.85	2.47; 2.40	2.44; 2.44	62	58
NiAs	3.93	3.91	2.67	2.64	69	92
h-BN[d]	3.81	3.69	2.42; 2.89	2.49; 2.71	62	63

Si-In

Crystal structure	E_{coh}(eV)		Bond length (Å)		B (GPa)	
	GGA	ps.1 & 2	GGA	ps.1 & 2	GGA	ps.1 & 2
ZnS	3.51	3.51	2.64	2.65	37	32
NaCl	3.54	3.53	2.82	2.86	47	57
CsCl	3.48	3.48	3.02	3.01	66	72
ZnO	3.50	3.51	2.66; 2.60	2.65; 2.65	48	32
NiAs	3.64	3.56	2.88	2.85	46	65
h-BN[e]	3.49	3.47	2.63; 3.03	2.66; 3.00	50	45

[a]Wurtzite and h-BN are hexagonal structures which are characterized by both a and c directions.
[b]For ZnO and NiAs are included, although they were not used in the fitting.
[c]The c/a value of 1.03582 for Si-As was kept constant during relaxation.
[d]The c/a value of 1.08846 for Si-Ga was kept constant during relaxation.
[e]The c/a value of 1.117 for Si-In was kept constant during relaxation.

Supplemental Material [19]) and the fitting procedure used to obtain Tersoff parameters for Si$-X$ interactions (where $X =$ In, Ga, or As) from the *ab initio* database of properties that we created for this purpose (Table I). We validate the parameter sets by their ability to reproduce commonly encountered thermodynamic properties such as cohesive energy, bond lengths, and elastic properties that were used in the parameter fitting (Sec. II). As a stronger test of these Tersoff models, we also present data for predictions of the "substitutional energy" of neutral Si dopants in InGaAs in comparison to our new *ab initio* predictions. Si dopants can be considered as "defects" in the InGaAs lattice, specifically as $\mathrm{Si}^0_{\text{In-Ga}}$ defects. Since Si is desired as a substitutional defect, this "defect formation energy" will be referred to as the substitutional energy. These predictions test the transferability and applicability of the Tersoff parameters to environments other than the ones to which they were fitted. Finally, we test the efficacy of these models by using them to investigate the effects of changing the composition of In or Ga atoms at 2nn positions surrounding a Si dopant on the substitution energy.

II. METHODOLOGY

A. Creation of an *ab initio* database

The quality of the parameters obtained for a given force field or interatomic potential model depends to a considerable extent on the quality of the reference database. For a bond-order-type interatomic potential model, like the Tersoff model, having as many crystal structures as possible as part of the reference database is desirable. However, some approximations should be also considered. Since the form of Tersoff model used in this paper takes into account only first nearest neighbors (1nn) and symmetry bonding, i.e., an A-B bond is the same as a B-A bond, only crystal structures that conform to this limitation were included in the reference database. Cubic structures (such as simple cubic, diamond, ZnS, NaCl, and CsCl) are symmetric and can be well described by a 1nn-based model; therefore, they are widely used for Tersoff parameter fitting. Simple cubic and diamond structures are mostly used for pure elements and are not included in this paper. Other common crystal structures for compound materials, such as wurtzite, NiAs, hexagonal-BN (h-BN) structures were also considered, but only h-BN passed our screening: Wurtzite behaves the same as ZnS under the 1nn approximation; NiAs has an asymmetric nature for its local bonding. Therefore, we are left with consideration of ZnS, NaCl, CsCl, and h-BN as our reference database for the parameter fitting process.

To create the reference *ab initio* database, we performed total energy calculations using a plane-wave density functional theory (DFT) code [20] with projector augmented wave (PAW) pseudopotentials that include nonlinear core corrections and scalar relativistic effects. The exchange and correlation term is described using a generalized gradient approximation (GGA) [21]. The Monkhorst-Pack scheme [22] is used to represent k-point meshes. For each system, we performed convergence tests on the total energy with respect to cut-off energy and the number of k points. The results of a test on system size dependence are given in the Supplemental Material [19].

As a verification of the quality of our DFT results, we compared simulated lattice constants of the pure elements (In-In, Ga-Ga, As-As) and thermodynamically stable binary alloys (GaAs and InAs) against known experimental values. This comparison generally shows good agreement between the DFT and experiment: The lattice constants agree within a roughly 3% difference in value. More significant differences (typically on the order of 1–2 eV) between our *ab initio* calculations and experimental results were observed for the cohesive energy of covalent bonded elements and binary alloys (Si, As, GaAs, and InAs). However, our predicted cohesive energies show very similar results to similar *ab initio* calculations derived from the MIT-based Materials Project [23,24]; see the results in Table S3 [19]. The tendency of *ab initio* DFT/GGA predictions to overbind III-V structures is well known [25]. For quantities involving energy differences such as surface and formation energies, we expect any systematic errors to be nullified, with typical differences of less than 0.2 eV. This difference between experiment and DFT predictions are discussed in Sec. III A (also shown in Table S3 [19]), where we compare our parameters to existing In-Ga-As parameter sets, which have been shifted by the amount necessary to match experimental data [26,27], as illustrated in Fig. 1. Scaling DFT values to match experiment showed no significant difference from using a shifting method [8]. The scaling approach was also used, and the modified parameters are shown in Tables S4 and S5 [19].

B. Parameter fitting procedure

While there is no standard procedure for fitting parameters involved in the formulation of a force field or interatomic potential model, there are several essential and necessary steps. The first requirement, in the absence of experimental data, is to create a comprehensive and reliable reference database of properties of the system being modeled. In the case of the Si-X interactions, no experimental data are available since

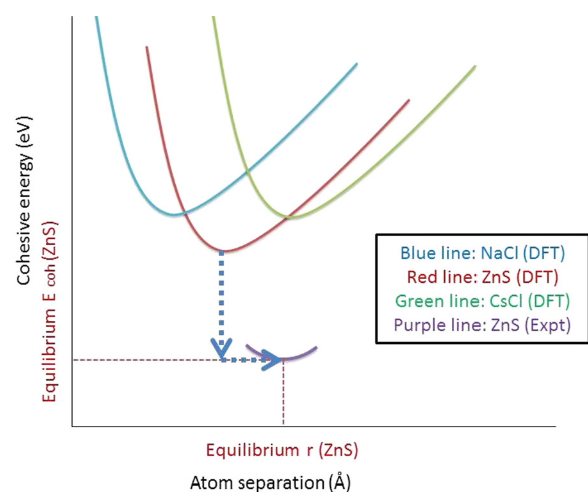

FIG. 1. (Color online) Schematic to represent the shifting of the DFT reference dataset to experimental data for equilibrium crystal structures. The lowest energy minimum and the corresponding equilibrium distance from DFT data are made equal to available experimental cohesive energy and bond length, respectively, in order to neglect the DFT offset from experiment.

Si-Ga and Si-In are theoretical compounds and Si-As has rarely been studied experimentally [28]. In such cases, it is necessary to create a reference database using first principles methods, principally DFT and GGA [21], as described in the preceding section. Cohesive energies and lattice constants were calculated by minimizing the energy of the system of interest (e.g., a given crystal structure) using Beeman's algorithm and the Wentzcovitch Lagrangian as implemented in Quantum Espresso [20]. The bulk modulus was calculated by fitting the equation of state to that for a Murnaghan formulation. The results are shown in Table I.

The second component involves the fitting procedure itself. We follow the approach used previously by Biswas and Hamann [29] and by Tersoff [10] and use a nonlinear least squares fit procedure (Levenberg-Marquardt algorithm using Genplot [30]). For the most general and commonly used form of the Tersoff model, there are 14 parameters. Of these 14, four of them can be found from experimental data: D_{ij} and $R_{ij}{}^0$ are the diatomic binding energy and equilibrium length, respectively. Two others, β_{ij} and S_{ij}, can be determined if enough experimental data are available [31]: β_{ij} can be determined if both D_{ij} and the ground state frequency are known. Also, S_{ij} can be determined from the Pauling relation [31]. However, in this case, since there are no experimental data, these four parameters remain free but should acquire values that do not lead to unphysical predictions, such as overly large diatomic binding energies or equilibrium bond lengths. This additional freedom to set four more variables may help us find a better fit to the reference data, but it can also result in multiple sets of parameters whose relevant merits must be evaluated. The n_{ij} parameter is set to 1 to be in agreement with the second-order momentum approximation. Here, γ_{ij} is an additional adjustable parameter, but was set to 1 in this paper following the procedure of Albe *et al.* [31]. Parameter m_{ij} can be set to either 1 or 3 in large-scale atomic/molecular massively parallel simulator (LAMMPS); it was set to 1 in this paper, following the procedure of Hammerschmidt *et al.* [8].

Parameters governing the cutoff functions for the Tersoff models are not included in the systematic fitting process, since determining the appropriate cutoff values to use is complicated. Most prior papers have followed Tersoff's original approach and assumed that the cutoff is made at a distance corresponding to the inclusion of 1nn for each crystal structure. Albe *et al.* took a different approach [31]: They chose to reproduce the melting point as the metric in determining a suitable value for the cutoff, but even this group did not include the cutoff in their fitting procedure. This paper follows the original Tersoff method and does not include the cutoff value in the fitting process. Here, the cutoff radius was chosen to lie between the equilibrium bond lengths of 1nn and 2nn of each crystal structures, i.e., ZnS, NaCl, CsCl, h-BN, and further determined by inclusion of the relaxed bond length of the Si dopant to its 1nn at all the defect positions of interest. All the equilibrium bond lengths were acquired from our DFT calculations.

Some of the parameters were fitted under certain constraints to prevent unphysical results. For example, h, which is analogous to $\cos\theta_{ijk}$, must lie in the range $-1 < h < 1$. Similarly, S_{ij} should not equal 1 to avoid infinite repulsion and attraction terms. The remaining parameters (γ_{ij}, c_{ij}, d_{ij}, μ_{ij}) are adjustable with no constraints. However, we found during the fitting process that the parameter μ_{ij}, which is mostly related to the h-BN structure, was extremely important in determining the defect formation energy, which is a prime concern to our proposed application for these models. The parameter μ_{ij} controls the resistance to stretch and the relative bond length for the connecting bonds. It is not only the μ_{ij} values of the binary Si-X models that matter, but also those of the In-As/Ga-As. Therefore, in order to be compatible with the existing In-Ga-As Tersoff model, the μ_{ij} values were separately adjusted so that they reproduced the correct trend in a set of defect formation energies that targeted Si-X interactions in a variety of different environments.

The results of the fitting to create viable parameter sets are shown in Table II. The first set of parameters (named "ps.1") not only fits bulk properties well, but also provided a qualitatively good prediction of the DFT results for defect formation energies. The last task involves a more stringent validation of the parameter set. Initially, we compared the results of the Tersoff model-generated results against the DFT reference database that we created and which was described above; see Table I. Since the three ps.1 Tersoff parameter sets for Si-Ga, Si-In, and Si-As (Table II) are each a best fit across all cubic crystal structures, it is not guaranteed that they will reproduce the *ab initio* data from which they were generated. Parameter sets are invariably a compromise between improving the reproduction of one structure, often at the expense of the reproduction of properties for another structure. The root mean square errors (RMSE) of the fit to all cubic structures are 0.10, 0.20, and 0.09 eV for Si-As, Si-Ga, and Si-In, respectively.

As a case in point, we provide (in Table II) an alternative parameter set (named "ps.2") with the same Si-Ga and Si-In interactions, but a different Si-As interaction. We found it was only necessary to modify the Si-As potential model to obtain a good fit to defect formation energies. The RMSE of this fit is calculated to be 0.13 eV. The Si-As potential of ps.2 was a broad fit to all four crystal structures selected above (i.e., including h−BN), instead of only cubic crystals in ps.1. Anticipating the results that follow, we shall show that the

TABLE II. Parameter sets for Si-X pairwise interaction. The RMSE of each fit is given in the bottom row.

	Si-As (ps.1)	Si-As (ps.2)	Si-Ga[a]	Si-In[a]
D_{ij}(eV)	4.79841	4.3381	3.124428	3.3719795
R^0_{ij}(Å)	2.13339	2.0978	2.1973155	2.3111975
S_{ij}	1.913203	1.26936	1.2005	1.3574872
β_{ij}(1/Å)	1.082611	1.13142	1.2789162	1.17268
δ_{ij}	0.271506	0.0952155	0.05845635	0.1356779
c_{ij}	1.640876	0.342903	0.53355	0.1811664
d_{ij}	0.9159	0.531886	0.655665	0.3842507
h_{ij}	−0.10111	−0.170953	−0.358167	−0.2569319
μ_{ij}(1/Å)	−1.19500	−0.415	−1.295	1.15
γ_{ij}	1.0	1.0	1.0	1.0
n_{ij}	1.0	1.0	1.0	1.0
m_{ij}	1.0	1.0	1.0	1.0
R^c_{ij}(Å)	3.2	3.2	3.2	3.3
D^c_{ij}(Å)	0.1	0.1	0.1	0.1
RMSE (eV)	0.10	0.14	0.20	0.09

[a]Parameters for Si-Ga and Si-In are identical for ps.1 and ps.2.

ps.2 models provide better values of the defect formation energies in *interstitial* environments than ps.1, but at the expense of failing to reproduce the DFT-generated trends that show comparable formation energies for cationic and anionic *substitutional* defects.

C. Validation: Prediction of defect formation energies

To validate the transferability of the best parameter set to properties that match our particular research interests, we also predict properties that were *not* included in the first fitting process. We chose to predict the defect formation energy due to its critical role in dopant activation, which was a primary motivation for us to create these Tersoff models. A set of neutral defect formation energies were calculated using DFT/GGA techniques in which a single Si atom was inserted into a number of different environments that can be found in the InGaAs matrix.

Using the Tersoff potentials for In, Ga, and As, we determined the energies of various $In_xGa_{1-x}As\,(x = 0.5)$ matrices (varying from perfect ordering of cations to complete randomness) and found variations in energy to be less than 15 meV per atom. This implies the absence of energetically preferred atomic coordination. This is in agreement with the random ordering observed for bulk semiconductors prepared at high temperatures [32]. However, epitaxially grown III-V alloys on substrates are known to exhibit specific ordering of the cations [33,34]. This ordering is induced at the surface during epitaxial growth due to kinetic constraints at step and ledge boundaries. Such ordered ternary alloys have higher energy and give rise to a split at the valence band maximum (VBM) and a lower energy of the conduction band minimum (CBM) relative to random ordering [35].

Given these experimental observations, we have also studied CuPt-B [36,37] and CuAu-I [4,38] ordering of the InGaAs alloy [39]. CuPt-B and CuAu-I ordering exhibit alternating In and Ga planes along the [111] and [100] directions, respectively. Domains of several types of ordered structures often coexist in III-V alloys [40,41]. Such structural defects are composed of antiphase boundaries and orientational domain boundaries, leading to spatial variations in the order parameter and some interesting optical effects [42–44]. It has been found that the presence of an impurity can induce disorder, e.g., a reported case involves $In_{0.5}Ga_{0.5}P$ when doped with Si or Se [45]. Therefore, we have also considered a random configuration of InGaAs for our studies, referred to simply as "random alloy." For simplicity and convenience, we have taken a 0.5:0.5 ratio for In and Ga. Schematics of all these three configurations are shown in Fig. S6 [19]. The three configurations in the following discussions refer to random ordering and CuPt-B and CuAu-I ordered structures.

Since there are no experimental values for defect formation energies in these systems, we had, once again, to construct a reference database generated from DFT/GGA calculations. To validate the DFT results, we first conducted a convergence test on the effect of the size of the supercell on the resulting energy, for systems ranging in size from 16 to 64 to 128 atoms. The results are shown in Table S7 [19]. A 64 atom box was chosen for all the remaining calculations, based on a tradeoff between accuracy and computational cost. The cell size error was estimated to be around 0.1–0.2 eV; similar error estimates were reported by Van de Walle [46]. A supercell of pure InGaAs was first fully relaxed using Beeman's algorithm with a Wentzcovitch Lagrangian. Then, we introduced a single Si atom into the supercell and relaxed the entire system with a fixed cell constant using the Broyden-Fletcher-Goldfarb-Shanno (BFGS) algorithm [47–49].

Next, we calculated the same set of defect formation energies using the Tersoff models we developed above. A similar procedure was implemented as for the DFT/GGA calculations except that LAMMPS [50] was used in combination with the Tersoff models. Periodic boundary conditions were used in all three Cartesian directions, as appropriate for a bulk system. An energy minimization of the simulation box was performed using the conjugate gradient (CG) algorithm. A comparison of the Tersoff-generated defect formation energies against the DFT/GGA-generated values for all three configurations is shown in Table III and will be discussed in the Results section.

The formalism for the defect formation energy depends on the chemical potential, as developed by Northrup [51], Zhang and Northrup [52], and Northrup and Zhang [53]. Lee and Chang [54] studied defect formation energies for a similar system, carbon-doped InGaAs. Thus, we can write an analogous equation for the substitutional defect formation energy in a Si-doped InGaAs as given by:

$$E_{\text{form}} = E'_D + Q_D \times \mu_e - \tfrac{1}{4}\,(n_{\text{In}} + n_{\text{Ga}} - n_{\text{As}})\,\Delta\mu \\ - \tfrac{1}{2}\,(n_{\text{In}} - n_{\text{Ga}})\,\delta\mu - n_{\text{Si}} \times \left(\mu_{\text{Si}} - \mu_{\text{Si}}^{\text{bulk}}\right), \quad (1)$$

where E'_D is the chemical potential-independent term, as defined below; Q_D is the charge of the defect; n_i is the number of atoms of element i in the supercell; μ_i is the chemical potential of elements which depend on the processing environment; μ_i^{bulk} is the chemical potential of the bulk thermodynamically stable element or compound, which is computationally equal to the total energy. The value of $(\mu_{\text{Si}} - \mu_{\text{Si}}^{\text{bulk}})$ should be smaller than zero, but will have no minimum constraint if no SiAs precipitation exists.

$$E'_D = E_D - \frac{1}{2}\left(n_{\text{In}} - \frac{n_{\text{As}}}{2}\right) \times \left(\mu_{\text{In}}^{\text{bulk}} - \mu_{\text{As}}^{\text{bulk}}\right) \\ - \frac{1}{2}\left(n_{\text{Ga}} - \frac{n_{\text{As}}}{2}\right) \times \left(\mu_{\text{Ga}}^{\text{bulk}} - \mu_{\text{As}}^{\text{bulk}}\right) \\ - \frac{1}{4}\,(n_{\text{In}} + n_{\text{Ga}} + n_{\text{As}}) \times \mu_{\text{InGaAs}_2}^{\text{bulk}} \\ - \frac{1}{4}\,(n_{\text{In}} - n_{\text{Ga}}) \times \left(\mu_{\text{In}}^{\text{bulk}} - \mu_{\text{Ga}}^{\text{bulk}}\right) - n_{\text{Si}}\mu_{\text{Si}}^{\text{bulk}}. \quad (2)$$

Here, $\Delta\mu$ and $\delta\mu$ are the upper and lower bounds for the energy, such that they define the range within which the energy of the system can change with respect to the chemical potential condition. They are defined below:

$$\Delta\mu = (\mu_{\text{In}} + \mu_{\text{Ga}} - 2\mu_{\text{As}}) - \left(\mu_{\text{In}}^B + \mu_{\text{Ga}}^B - 2\mu_{\text{As}}^B\right), \quad (3)$$

where

$$-\Delta H_f^{\text{InGaAs}_2} \leqslant \Delta\mu \leqslant \Delta H_f^{\text{InGaAs}_2} \quad (4)$$

TABLE III. Formation energy of neutral defects calculated from *ab initio* and Tersoff models. Immediate cation neighbors of Si are given in parenthesis for Si_{As}, Si_{T1}, and Si_{T2} defects.

	Configuration 1 (random alloy)			Configuration 2 (CuPt-B ordering)			Configuration 3 (CuAu-I ordering)		
Defect	GGA	ps.1	ps.2	GGA	ps.1	ps.2	GGA	ps.1	ps.2
Substitutional defects									
Si_{Ga} (Si on a Ga site)	0.96	1.12	0.57	0.98	1.12	0.59	0.98	1.22	0.58
Si_{In} (Si on an In site)	0.98	0.95	0.47	0.52	0.69	0.15	0.73	0.78	0.38
Si_{As} (Si on an As site)		(2Ga, 2In)			(3Ga, 1In)			(2Ga, 2In)	
	0.90	0.87	0.87	0.69	0.83	0.83	0.88	0.89	0.89
					(1Ga, 3In)				
				0.89	1.00	1.00			
Interstitial defects									
Si_{T1}[a] (Si atom in a tetrahedral, T1, site)		(3Ga, 3In)			(3Ga, 3In)			(4Ga, 2In)	
	3.24	1.43	1.44	3.02	1.50	1.54	3.02	1.99	1.90
								(2Ga, 4In)	
							3.12	2.42	1.22
Si_{T2}[b] (Si atom in a tetrahedral, T2, interstitial site)		(2Ga, 2In)			(3Ga, 1In)			(2Ga, 2In)	
	3.30	7.77	2.48	2.97	5.78	1.43	3.17	6.77	2.47
					(1Ga, 3In)				
				3.23	6.47	2.57			

[a]T1 site indicates an interstitial site located at the center of the anion tetrahedron.
[b]T2 site indicates an interstitial site located at the center of the cation tetrahedron.

and

$$\delta\mu = (\mu_{\mathrm{In}} - \mu_{\mathrm{Ga}}) - \left(\mu_{\mathrm{In}}^{B} - \mu_{\mathrm{Ga}}^{B}\right), \tag{5}$$

where $-\frac{1}{2}(\Delta H_f^{\mathrm{InGaAs_2}} - \Delta\mu) \leqslant \delta\mu \leqslant \frac{1}{2}(\Delta H_f^{\mathrm{InGaAs_2}} - \Delta\mu)$, where $\Delta H_f^{\mathrm{InGaAs_2}}$ is $\mu_{\mathrm{In}}^B + \mu_{\mathrm{Ga}}^B + 2\mu_{\mathrm{As}}^B - \mu_{\mathrm{InGaAs_2}}$.

It should be noted that it is only possible to consider comparisons between the *ab initio* data and the Tersoff model predictions for noncharged defects. Semiempirical models, such as Tersoff, cannot describe the behavior of charged defects. It should also be noted that we shift the energy predicted by the Tersoff parameter sets for In-Ga-As in order to match our DFT calculations of the cohesive energy.

D. Test case: Microsegregation of Ga/In 2nn's of Si on cationic lattice sites

In order to test the hypothesis that the local environment around a Si atom will affect its preference for a lattice site, we chose to explore the most extreme versions of the nature of the 12 2nn's of the Si atom. Thus, we considered systems in which the 2nn's of the Si atom were either all Ga or all In atoms. The remainder of the InGaAs matrix was a random alloy of In and Ga cation sites. The total numbers of Ga and In atoms are kept constant approximately at 50 In and 50 Ga per 100 As atoms. This is represented in Fig. 2 as the pathway from II to IV. We chose configuration 1 of InGaAs for this paper since it has the most randomly arranged set of In/Ga atoms, and this configuration has the lowest energy among all the configurations used in this study. Thus, using the random configuration 1 prevents introducing strain energy into the system by ordering the In and Ga atoms.

We also compare the energy of pure InGaAs for a random configuration 1 (situation I in Fig. 2) with the energy of InGaAs corresponding to microsegregation of In or Ga to occupy all 2nn sites (situation III in Fig. 2). This energy difference is defined as the strain energy in this paper.

$$E_{\mathrm{strain}} = E\,(\mathrm{III}) - E\,(\mathrm{I})\,.$$

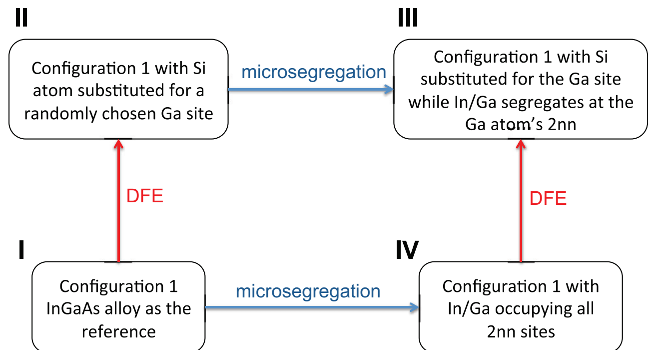

FIG. 2. (Color online) Decoupling the effects of strain energy and defect formation energy (DFE) using a set of pathways that explore the net effect of microsegregation. Situation I describes the randomly arranged pure InGaAs alloy displayed by configuration 1 (random alloy). Situation II has one randomly chosen Ga site replaced by a Si atom. Situation III describes the local microsegregation of In/Ga at the 2nn sites of a (randomly chosen) chosen Ga site. Situation IV has the chosen Ga site (in situation III) replaced by Si with the 2nn occupied by all In or Ga atoms.

To be more comprehensive, the defect formation energies of different scenarios (from situation I to II vs from III to IV) are also estimated.

III. RESULTS

A. Test of the DFT reference data against known experimental data and prior DFT results for binary III-V systems

As a test of our reference DFT/GGA database, we compared results for the cohesive energy, bond length, and unit cell parameters (a, b, c) for well-established and thermodynamically stable elemental systems (Si, Ga, In, As) and binary compounds (GaAs and InAs) against existing experimental data and prior DFT results. These results are tabulated in Table S3 [19]. Our DFT calculations show excellent agreement with prior DFT calculations, most within ∼1% difference. On those occasions where larger differences were found in comparison to prior DFT results, our calculations are generally closer to the experimental data. Comparing our calculations with experimental data, the lattice parameters show excellent agreement with experiment. The relative difference is less than 2%, which is below the residual error bar reported by Lejaeghere *et al.* [55]. However, for the cohesive energy, the level of agreement between experiment and our DFT predictions fall into two categories: For metallic bonding, such as In and Ga, we find excellent agreement with experiment, with differences smaller than 0.1 eV. On the other hand, for covalently bonded materials, the absolute differences are large, about ∼1.5 eV for GaAs, InAs, and As and ∼0.8 eV for Si. However, large differences are also observed in the DFT calculations of other authors, which seem to point to an inherent error of DFT/GGA. Care is required when comparing values of the cohesive energy from existing Tersoff models, whose reference data are shifted to fit the experimental data, with the Si-*X* Tersoff models developed here, which are based only on our DFT reference database, as mentioned in Sec. II C. Figure 1 provides a pictorial representation of the scaling approaches. It was reported by Hammerschmidt *et al.* [8] that the difference between scaling by taking a ratio or by shifting is within the accuracy of the parameter fitting. Therefore, either approach should give comparable outcomes.

B. Validation of Tersoff models against our reference DFT data

Since we fitted our Si-*X* Tersoff models to a number of different crystal structures, the parameter set is, of necessity, something of a compromise. Accordingly, the chosen parameter set will not necessarily reproduce all the reference data used in the fitting. Therefore, our first test of the parameter sets for Si-*X* involved comparing properties against our calculated DFT/GGA reference data set. As shown in Table I, values of the bond length and cohesive energy generated by our Tersoff models agree very well with the DFT results. The average differences between Tersoff predictions and DFT results for the cohesive energy are generally small ($<1\%$), 0.05–0.06 eV, across the three interactions (Si-As, Ga-Si, and In-Si). The one exception is the *h*-BN structure whose properties were compromised in order to obtain the correct trend in defect formation energies when combined with existing In-Ga-As Tersoff models. Even for the (not-included) NiAs structure, the differences are less than 4% across the three Si-*X* interactions. The relative residual error in the DFT results themselves range from 1% (for As) to 9% (for In) [55].

Differences in bond length predictions between Tersoff and DFT are 0.02–0.04 Å, less than 2% on average. This compares well to the relative residual errors in DFT of these constituent atoms of 1–3% [55]. Predictably, the bulk modulus *B* differs more significantly between this Tersoff parameter set and DFT.

The determination of the bulk modulus *B* requires that the curvature of energy-volume space be captured correctly and hence is numerically sensitive. For example, Lejaeghere *et al.* [55] estimate the DFT prediction of *B* to have a relative residual error against experiment of 8% for Si, 16% for Ga and In, and 35% for As. The average difference between the Tersoff prediction and DFT results for bulk modulus ranges from 3–15 GPa (5–20%) for Si-As, 15–40 GPa (25–70%) for Si-Ga, and 5–20 GPa (10–40%) for Si-In. However, these differences fall within the uncertainty in the DFT results themselves.

Overall, the comparison of DFT to Tersoff is within error predictions for DFT/GGA itself. The lattices we tested cover a range of structures, from expected arrangements, like zinc blende, to rarer structures. Comparison of Tersoff-derived values suggests that the ps.1 and ps.2 parameter sets are acceptably good.

C. A global test case: Enthalpy of formation of InGaAs from mixing of InAs and GaAs

Each individual InGaAs configuration has a different local arrangement of cations, leading to different angular terms in the Tersoff potential. This unique choice of angular terms for each configuration controls the global strain in the system. Enthalpy is a strong indicator of strain, and hence, we have calculated the enthalpy of mixing of InAs and GaAs for the formation of the random, CuPt-B, and CuPt-I configurations of $In_{0.5}Ga_{0.5}As$. The DFT-GGA calculations on a 64 atom unit cell of InGaAs give enthalpies of 3.08, 10.99, and 7.59 kJ/mol for random, CuPt-B, and CuPt-I configurations, respectively. Enthalpies of 2.60 and 2.94 kJ/mol have been reported in the literature based on *ab initio* calculations and tin solution calorimetry measurements, respectively [56]. Our random configuration shows a reasonable agreement with those values. The positive values of enthalpies indicate possible miscibility gaps [39]. However, the kinetic constraints at the substrate surfaces forbid phase-separated domain formation and pave the way for the formation of ordered alloys. It is to be noted that we have not considered any influence of the substrate in our calculations. The differences in the enthalpies of formation of CuPt-B and CuAu-I arrangements show that the strain is developed differently when alternate In/Ga planes orient along [111] or [100] planes. Experimentally, such directions are selected based on the substrate orientation. Our Tersoff model calculations (using ps.1) on a much larger 4096 atom unit cell show similar trends for random, CuPt-B, and CuAu-I configurations; the enthalpies are 4.65, 11.66, and 5.54, respectively. These results provide evidence that our model can reproduce the effect of nontrivial cation distributions on the total strain of the system, and the model can be carried forward to the calculation of dopant energetics in different environments with confidence.

D. Prediction of the formation energy of neutral defects

In order to test the transferability of our Tersoff models, we constructed a more stringent test by predicting a property that was not included in the fitting process described above. This test is not completely predictive since $\mu_{\rm ij}$ was adjusted in order to determine the right trend for defect formation energies. As mentioned above, this test also necessitated the creation of a new set of reference DFT data to compare to the Tersoff predictions.

The defect formation of a compound material depends on the chemical potential. Since we only consider neutral defects in this paper, the chemical potential of the electron is ignored ($\mu_e = 0$). For the discussion that follows, we choose conditions that are Si-, Ga-, and In-rich, i.e., $(\mu_{\rm Si} - \mu_{\rm Si}^{\rm bulk}) = 0$, $\Delta\mu = \Delta H_f^{\rm InGaAs_2}$, and $\delta\mu = 0$.

The Tersoff-generated and DFT-predicted results of the defect formation energies for a variety of different defects are shown in Table III. The DFT results predict that the *substitutional* defect the most likely to form is one in which Si replaces an In atom in the lattice (i.e., it has the smallest formation energy). However, as we shall show later, this tendency was found to result from the introduction of strain energy induced by having an orderly arrangement of In and Ga atoms on cationic lattice sites. Therefore, as expected, in configuration 1, in which In and Ga atoms are randomly arranged, there is no preference for Si to replace either an In or a Ga atom on a lattice site. On the other hand, for configurations 2 and 3 (CuPt-B and CuAu-I, respectively), which have layered structures along certain directions, the substitution of Si for In is favored due to the release of strain energy as Si is a smaller atom than In. Si requires almost the same amount of energy to replace a Ga in random and ordered configurations. Defects in which Si replaces an anionic As atom in a Ga-rich environment are 0.2 eV more favored than the case in an In-rich environment. Overall, our results suggest that the *substitutional* formation energies approximately lie in the range from 0.5 and 1.0 eV, whether Si induces disorder or not, or whether Si sits at a domain boundary.

For situations in which Si atoms occupy *interstitial* locations, our DFT calculations predicted that the formation energies are substantially higher than those of *substitutional* defects. All the interstitial defects in tetrahedral sites (T1 and T2: tetrahedral centers of anions and cations, respectively) give rise to essentially the same formation energy. All the hexagonal interstitial defects are unstable and diffuse back to tetrahedral interstitial sites. The differences among them are generally within the error of the defect formation energy calculations.

As shown in Table III and in Figs. 3 and 4, our first Tersoff parameter set, ps.1, generally predicts a value ~0.1 eV higher for the formation energy of the cation *substitutional* defect than the corresponding DFT calculation, generally the same order for the formation energy of an anion substitutional defect, and ~1.3 eV lower for the energies of the T1 *interstitial* defects. The T2 *interstitial* defects were the least well predicted, generally ~3.5 eV higher than their DFT counterparts for the defect formation energies. This tendency for Tersoff models to predict higher formation energies is well known; for example, in similar studies for GaAs [57], differences of 0.5–3.0 eV are not uncommon. In comparison, the ps.2 parameter sets predict

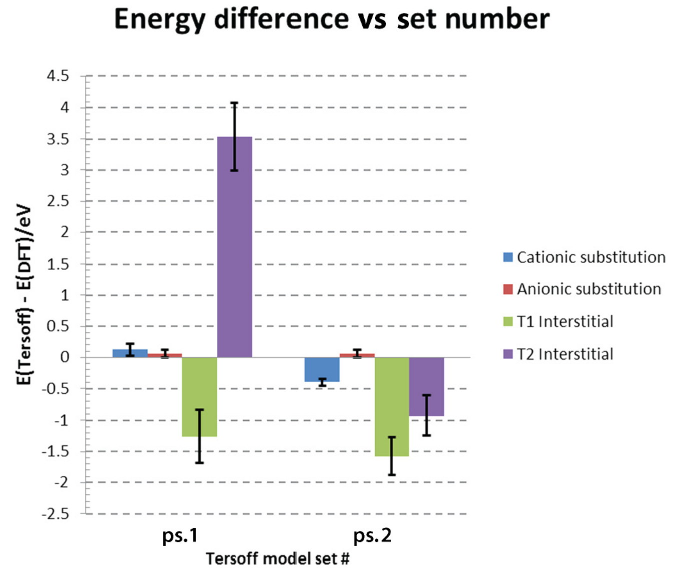

FIG. 3. (Color online) Energy differences between predictions of the Tersoff potential models and our DFT calculations for defect formation energies. Results are shown for two sets of Tersoff parameters (ps.1 and ps.2) and for four defect categories: cationic and anionic substitutional sites (blue and red, respectively) and for two types of interstitials, T1 and T2 (green and purple, respectively). Ps.1 does better at predicting defect formation energies from substitutional sites; ps.2 is substantially better at predicting T2-type interstitials but does slightly worse for the substitutional sites.

a value ~0.4 eV lower for the formation energy of the cationic *substitutional* defects than the corresponding DFT calculation. Since the anionic defect formation energy is controlled by the Si-Ga and Si-In interactions, which are the same for ps.1 and ps.2, the result is the same for both parameter sets. The defect formation energies predicted by ps.2 are ~1.6 eV lower for T1 interstitial defects and ~0.9 eV lower for T2 interstitial defects than corresponding DFT calculations.

Differences in the substitutional defect formation energy for ps.1 may be attributed to RMSEs of up to 0.20 eV in the fit

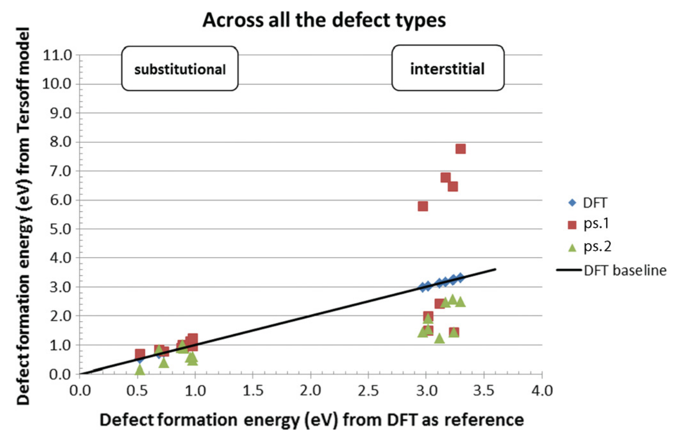

FIG. 4. (Color online) Scatter chart of Tersoff-generated defect formation energy against DFT-generated defect formation energy values. Ps.1 (red dots) predicts a better trend for substitutional defects, while ps.2 (green dots) predicts a better trend for interstitial defects.

TABLE IV. Strain energies and defect formation energies corresponding to the pathways illustrated in Fig. 2. The effect of strain energy introduced by microsegregation is shown in rows two (I → III) and three (II → IV). The data show that strain energy is significant. The effect of the defect formation energy is shown in row four (I → II and III → IV). Results show that the defect formation energy is essentially the same in random (column 1) and microsegregated environments (columns two and three), within the uncertainty in the calculations. The first row shows the energy differences compared to the reference situation I, i.e., it includes strain and formation energies. It can be seen that the sum of the strain and formation energies (rows two or three with row four) is essentially the same as that in row one. The defect under discussion is Si_{Ga}.

Pathway (energy)	Configuration 1 (random alloy)[a]	Ga segregation at 2nn[a]	In segregation at 2nn[a]
I → II or IV (strain + formation)	1.10 eV	2.65	1.83
I → III (strain)	0.00 eV (reference)	+1.64 eV	+0.78 eV
II → IV (strain)	0.00 eV (reference)	+1.55 eV	+0.73 eV
I → II (III → IV) (formation)	1.10 eV	1.01eV	1.05 eV

[a]All these studies were made using a 4096 atom simulation box.

(see Table II). For the Si_{As} defect, Si is bonded only to In and Ga; therefore, ps.1 and 2, which differ only in the fitting of Si-As, give identical results. In the cases of Si_{In} and Si_{Ga} defects, Si is only bonded to As; therefore, the Si-As fitting is significant. However, as a result of the high RMSE for the Si-As zinc blende geometry, a large deviation from DFT is obtained. On the contrary, for interstitial defects, the angular environment of Si cannot be replicated by the zinc blende geometry of Si-X alone; therefore, the choice of crystal structures for fitting would have an impact on the difference from DFT results, in addition to an error related to the fitting process.

Echoing the DFT results, ps.1 also predicts that the substitutional defect in which Si replaces In is the more energetically favorable cationic substitution, but the Tersoff model has a small but systematic preference for the *anionic* substitutional defect of ~0.05 eV. On the other hand, although ps.2 has a systematic preference for the *cationic* substitutional defect by ~0.45 eV, it still predicts that substitutional defects in which Si replaces In are the most energetically favorable change. For the comparison between interstitial and substitutional defects, both ps.1 and ps.2 predict that Si dopants in interstitial lattice sites are substantially less energetically favored compared to Si dopants in substitutional lattices. For substitutional defects, ps.2 reproduced the variation and trend with respect to ordering shown in DFT.

In summary, the ps.1 and ps.2 parameter sets have predicted the right trends across all the defect categories and configurations we studied. They should thus be suitable for the next task, finding the most probable local environment around Si in an InGaAs alloy.

E. Model application test case: Effect of local composition on defect formation energy

Since the Tersoff models developed in this paper were shown to be capable of an acceptably accurate representation of the DFT results, we applied these models to the task of identifying the most probable local environments around Si dopants in InGaAs alloys. As a first step, we determined whether the substitutional energy for a Si dopant was influenced by its local (2nn) environment.

This hypothesis was tested by comparing the defect formation energy that results from substituting a Si atom for a Ga atom in configuration 1 (random) and then altering the nature of its immediate environment (2nn). Thus, we take a randomly substituted $In_{0.50}Ga_{0.50}As$ alloy (configuration 1) and make a single Si substitution for a Ga atom. Then, we study the effect of what might be termed local "microsegregation" by altering the In/Ga ratio of the 12 2nn's of the chosen Ga site. Nevertheless, we kept the global stoichiometry constant by changing the Ga/In ratio of cations farther away. For this test, we chose to study two extreme cases in which all 12 2nn's are either In or Ga atoms. The energies of both these environments, compared to a completely random arrangement of In/Ga 2nn's, will then provide information about the effects of microsegregation on the substitution of Si dopants (i.e., the defect formation energy).

The results shown in Table IV show that even this extreme hypothetical microsegregation of In/Ga does not affect the resultant formation energy; the difference in formation energies across all the columns is within the intrinsic uncertainty of the underlying techniques (0.1–0.2 eV). However, microsegregation will introduce considerable strain energy into the system: As shown in row 2 of Table IV (the pathway from I to III) and row 3 (the pathway from II to IV), the strain energy introduced by either Ga or In segregation to 2nn positions is significant, about 1.6 and 0.7 eV for Ga or In microsegregation, respectively. In contrast, the three entries in row 4 of Table IV show that there is no significant difference in formation energies whether the 2nn's are random (configuration 1), or all Ga, or all In. Taken together, we conclude that microsegregation will introduce some strain energy into the system, but will not alter the preference of Si for its choice of lattice site.

Global ordering imposes a significantly larger strain than microsegregation of cations around a dopant site in a random alloy. The 4096 atom cells of CuAu-I and CuPt-B configurations have strain energies of 9.39 and 74.41 eV, respectively, with respect to the random alloy. Microsegregation of In/Ga atoms at 2nn cation sites still leaves the 4096 atom cell somewhat random because those cation sites are equidistant radially from the dopant site and also because the stoichiometry is the same as the random alloy. It can be assumed that the strain acting on each atom in a random alloy is not necessarily the same due to the distinct local and global neighborhoods. For the CuAu-I and CuPt-B configurations, however, the strain acting on atoms on identical Miller planes is the same. Substitution of an atom by Si in either

configuration leaves some additional strain on Si due to the smaller Si-X (X = In, Ga, As) bond length compared to X-X. Since the equation for the formation energy indirectly contains the difference between the total energies of defected and nondefected systems [which are, respectively, brought in by the terms E_D and $\mu^{\text{bulk}}_{\text{InGaAs}_2}$ in Eq. (2)], it may be argued that how much of this strain attenuates through neighboring bonds determines the defect formation energy. Due to the reasonably good comparison between DFT and Tersoff results, this can be taken as the classical interpretation of neutral defect formation energy. Note that each atom cannot "see" the identity of 2nn and higher neighbors. Therefore, the strain attenuates through the bond strengths and bond angles of neighbors.

Like the DFT results shown in the previous section, the Tersoff models predict that microsegregation of cations around a dopant atom will not affect the defect formation energy. The Tersoff models also predict that the local ordering of In or Ga implied by this microsegregation can make In cationic lattice sites more favored than Ga sites due to the release of strain energy. This suggests that local ordering in InGaAs alloys may affect dopant diffusion due to the creation of localized strain.

IV. CONCLUSIONS

Two sets of Tersoff parameters have been developed to represent Si-X interactions (where X = Ga, In, As); these two sets differ in the weighting placed on different crystal structures. Both parameter sets represent a best fit to a range of crystal structures. They show strong consistency with the DFT/GGA reference dataset for at least zinc blende and rock salt structures, with results mostly within the known intrinsic errors of the DFT/GGA method itself. Overall, the errors of our Tersoff model are less than 1% for cohesive energy, less than 2% for bond length, and less than 30% for most of the bulk modulus values.

Parameter sets ps.1 show formation energies for cationic and anionic *substitutional* defects that are very close to DFT/GGA predictions, at the expense of worse prediction of some interstitial defects. Generally speaking, ps.1 has the ability to predict the right trend among different categories of defects and within *substitutional* defects. The alternative parameter set, ps.2, obtained by developing a new Si-As interaction with an adjusted μ_{ij} (but leaving the Si-Ga and Si-In potentials unchanged from ps.1), is substantially better at predicting T2-type interstitials, but does slightly worse for the substitutional sites. For the simulation of kinetic properties, the ps.2 parameter set is likely to be a more judicious choice due to its improved reproduction of the interstitial defects relative to ps.1.

Our paper on microsegregation effects shows that, for extreme cases in which all the 2nn's of a dopant are all the same type of cation (In or Ga), such segregation will introduce significant strain energy into the system as Si atoms will preferentially replace In. Taking into account the ordering of 2nn's, and the neighbors beyond that, the substitutional formation energy can vary by up to 0.5 eV (Table III). These results point to an important role for strain energy to affect the local composition around dopant atoms. Thus, strain energy release may play an important role on dopant diffusion and hence the extent of dopant activation.

Our results suggest that the first set of Tersoff parameters (ps.1) should work well for finding the most probable local environment around Si, but its overprediction of the formation energy of the T2 interstitial defect may deleteriously affect its ability to predict the migration energy and other kinetic properties. However, to quote Murdick's [57] assessment of the Tersoff model to predict defect formation energy predictions in GaAs: "For a wide range of processing conditions, there is no potential that is clearly superior [to Tersoff]." Finally, we remind readers that Tersoff potential models are appropriate only for neutral defects moving through the matrix of the material. Unlike the In-Ga-As parameters of Hammerschmidt *et al.* [8], which were originally fitted to bulk and surface properties, care must be taken when using our Si-In,Ga,As parameters for surface properties to which they were not fitted.

ACKNOWLEDGMENTS

CWL would like to thank Dr. Michelle Johannes (Naval Research Laboratory [NRL]) for her invaluable help regarding the formulation of expressions for the defect formation energy given in this paper. The authors thank Dr. Phil Oldiges and Dr. Pranita Kulkarni (IBM) for sharing important insights regarding dopant diffusion in InGaAs. This research was supported by the Semiconductor Research Corporation's Global Research Collaboration Task No. 2272.001. Computing resources were provided by the Cornell Institute for Computational Science and Engineering, supported by equipment donations from Intel and capital equipment funding from Cornell's Center for Materials Research, a National Science Foundation (NSF) funded Materials Research Science and Engineering Center (MRSEC) (DMR-1120296).

[1] T. P. Pearsall and J. P. Hirtz, J. Cryst. Growth **54**, 127 (1981).
[2] P. Clarke, "Intel's Gargini pushes III-V-on-silicon as 2015 transistor option," EE Times (2010). Available: http://www.eetimes.com/document.asp?doc_id=1173048
[3] "International Technology Roadmap for Semiconductors 2012 Update Overview", ITRS (2012). Available: http://www.itrs.net/Links/2012ITRS/2012Chapters/2012Overview.pdf
[4] O. Ueda, Y. Nakata, T. Nakamura, and T. Fujii, J. Cryst. Growth **115**, 375 (1991).
[5] Y. Fedoryshyn, M. Beck, P. Kaspar, and H. Jaeckel, J. Appl. Phys. **107**, 93710 (2010).
[6] K. R. Evans, J. Vac. Sci. Technol. B. Microelectron. Nanometer Struct.: Process., Meas., Phenom. **13**, 1820 (1995).
[7] S. J. Pearton, J. M. Kuo, W. S. Hobson, E. Hailemarian, F. Ren, A. Katz, and A. P. Perley, MRS Online Proc. Libr. **240**, (1991).
[8] T. Hammerschmidt, P. Kratzer, and M. Scheffler, Phys. Rev. B **77**, 235303 (2008).

[9] J. Tersoff, Phys. Rev. Lett. **56**, 632 (1986).
[10] J. Tersoff, Phys. Rev. B **37**, 6991 (1988).
[11] J. Tersoff, Phys. Rev. B **38**, 9902 (1988).
[12] J. Tersoff, Phys. Rev. B **39**, 5566 (1989).
[13] R. Smith, Nucl. Instruments Methods Phys. Res., Sect. B **67**, 335 (1992).
[14] M. Sayed, J. H. Jefferson, A. B. Walker, and A. G. Cullis, Nucl. Instruments Methods Phys. Res., Sect. B **102**, 218 (1995).
[15] P. A. Ashu, J. H. Jefferson, A. G. Cullis, W. E. Hagston, and C. R. Whitehouse, J. Cryst. Growth **150**, 176 (1995).
[16] K. Nordlund, J. Nord, J. Frantz, and J. Keinonen, Comput. Mater. Sci. **18**, 283 (2000).
[17] D. Powell, M. A. Migliorato, and A. G. Cullis, Phys. Rev. B **75**, 115202 (2007).
[18] H. Detz and G. Strasser, Semicond. Sci. Technol. **28**, 85011 (2013).
[19] See Supplemental Material at http://link.aps.org/supplemental/10.1103/PhysRevB.91.094108 for the detailed descriptions of Tersoff potential and defect formation energy, the developed parameters, the InGaAs structure models, and convergence of DFT formation energy with respect to cell size.
[20] P. Giannozzi, S. Baroni, N. Bonini, M. Calandra, R. Car, C. Cavazzoni, D. Ceresoli, G. L. Chiarotti, M. Cococcioni, I. Dabo, A. Dal Corso, S. de Gironcoli, S. Fabris, G. Fratesi, R. Gebauer, U. Gerstmann, C. Gougoussis, A. Kokalj, M. Lazzeri, L. Martin-Samos *et al.*, J. Phys.: Condens. Matter **21**, 395502 (2009).
[21] J. P. Perdew, K. Burke, and M. Ernzerhof, Phys. Rev. Lett. **77**, 3865 (1996).
[22] H. J. Monkhorst and J. D. Pack, Phys. Rev. B **13**, 5188 (1976).
[23] A. Jain, S. P. Ong, G. Hautier, W. Chen, W. D. Richards, S. Dacek, S. Cholia, D. Gunter, D. Skinner, G. Ceder, and K. A. Persson, APL Mater. **1**, 11002 (2013).
[24] A. Jain, G. Hautier, S. P. Ong, C. J. Moore, C. C. Fischer, K. A. Persson, and G. Ceder, Phys. Rev. B **84**, 045115 (2011).
[25] S. Sanvito, G. Theurich, and N. A. Hill, J. Supercond. **15**, 85 (2002).
[26] C. Kittel, in *Introduction to Solid State Physics*, 8th ed. (John Wiley & Sons, Hoboken, 2005), p. 680.
[27] *Handbook of Semiconductor Silicon Technology*, edited by William C. O'Mara, Robert B. Herring, and Lee P. Hunt (NOYES Publications, Park Ridge, New Jersey, 1990), p. 795.
[28] O. Madelung, U. Rössler, and M. Schulz, eds., *Non-Tetrahedrally Bonded Elements and Binary Compounds I* (Springer-Verlag, Berlin/Heidelberg, 1998).
[29] R. Biswas and D. R. Hamann, Phys. Rev. Lett. **55**, 2001 (1985).
[30] Comput. Graph. Serv. (Genplot), Available: http://www.genplot.com/
[31] K. Albe, K. Nordlund, J. Nord, and A. Kuronen, Phys. Rev. B **66**, 035205 (2002).
[32] J. C. Woolley, in *Compound Semiconductors* (Reihnhold, New York, 1962), p. 3.
[33] A. Zunger and S. Mahajan, in *Handbook of Semiconductors*, 2nd ed. (Elsevier, Amsterdam, 1994), p. 1439.
[34] T. P. Pearsall and G. B. Stringfellow, MRS Bull. **22**, 16 (1997).
[35] S.-H. Wei and A. Zunger, Phys. Rev. B **57**, 8983 (1998).
[36] A. Gomyo, T. Suzuki, K. Kobayashi, S. Kawata, I. Hino, and T. Yuasa, Appl. Phys. Lett. **50**, 673 (1987).
[37] D. J. Arent, M. Bode, K. A. Bertness, S. R. Kurtz, and J. M. Olson, Appl. Phys. Lett. **62**, 1806 (1993).
[38] T. S. Kuan, T. F. Kuech, W. I. Wang, and E. L. Wilkie, Phys. Rev. Lett. **54**, 201 (1985).
[39] A. Mascarenhas, ed., *Spontaneous Ordering in Semiconductor Alloys* (Kluwer Academic/Plenum Publishers, New York, 2002).
[40] S. R. Kurtz, J. Appl. Phys. **74**, 4130 (1993).
[41] Y. Zhang and A. Mascarenhas, Phys. Rev. B **55**, 13100 (1997).
[42] U. Dörr, H. Kalt, D. J. Mowbray, and C. C. Button, Appl. Phys. Lett. **72**, 821 (1998).
[43] H. M. Cheong, A. Mascarenhas, J. F. Geisz, J. M. Olson, M. W. Keller, and J. R. Wendt, Phys. Rev. B **57**, R9400 (1998).
[44] M. C. DeLong, W. D. Ohlsen, I. Viohl, P. C. Taylor, and J. M. Olson, J. Appl. Phys. **70**, 2780 (1991).
[45] A. Gomyo, H. Hotta, I. Hino, S. Kawata, K. Kobayashi, and T. Suzuki, Jpn. J. Appl. Phys. **28**, L1330 (1989).
[46] C. G. Van de Walle, J. Appl. Phys. **95**, 3851 (2004).
[47] R. Fletcher, in *Practical Methods of Optimization* (John Wiley & Sons, New York, 1987), pp. 285–286.
[48] S. R. Billeter, A. J. Turner, and W. Thiel, Phys. Chem. Chem. Phys. **2**, 2177 (2000).
[49] S. R. Billeter, A. Curioni, and W. Andreoni, Comput. Mater. Sci. **27**, 437 (2003).
[50] S. Plimpton, J. Comput. Phys. **117**, 1 (1995).
[51] J. E. Northrup, Phys. Rev. Lett. **62**, 2487 (1989).
[52] S. B. Zhang and J. E. Northrup, Phys. Rev. Lett. **67**, 2339 (1991).
[53] J. E. Northrup and S. B. Zhang, Phys. Rev. B **47**, 6791 (1993).
[54] S.-G. Lee and K. J. Chang, Phys. Rev. B **53**, 9784 (1996).
[55] K. Lejaeghere, V. Van Speybroeck, G. Van Oost, and S. Cottenier, Crit. Rev. Solid State Mater. Sci. **39**, 1 (2014).
[56] I. Ansara, O. Bodak, C. Chatillon, W. Chong, V. Tomashik, and A. Watson, in *Non-Ferrous Metal Ternary Systems. Semiconductor Systems: Phase Diagrams, Crystallographic and Thermodynamic Data*, edited by G. Effenberg, and S. Ilyenko (Springer-Verlag, Heidelberg, 2006), p. 159.
[57] D. A. Murdick, Ph.D. thesis, University of Virginia, 2006.